Geomorphology 302 (2018) 20–34

Contents lists available at ScienceDirect

Geomorphology

journal homepage: www.elsevier.com/locate/geomorph

Are equilibrium multichannel networks predictable? The case of the regulated Indus River, Pakistan

Carling P.A. [a,c,*], Trieu H. [a,1], Hornby D.D. [b], Huang He Qing [d], Darby S.E. [a], Sear D.A. [a], Hutton C. [b], Hill C. [b], Ali Z. [e], Ahmed A. [e], Iqbal I. [e], Hussain Z. [f]

[a] Geography and Environment, University of Southampton, Southampton, UK
[b] GeoData, Geography and Environment, University of Southampton, Southampton, UK
[c] College of Environment and Planning, Henan University, Keifeng, Henan Province 475004, China
[d] Key Laboratory of Water Cycle and Related Land Surface Processes, Institute of Geographical Sciences and Natural Resources Research, Chinese Academy of Sciences, Beijing 100101, China
[e] Pakistan Space and Upper Atmosphere Research Commission (SUPARCO), Islamabad, Pakistan
[f] Water Power and Development Authority, Islamabad, Pakistan

ARTICLE INFO

Article history:
Received 15 May 2017
Received in revised form 18 September 2017
Accepted 19 September 2017
Available online 27 September 2017

Keywords:
Indus River: river bank erosion
Channel stability
Anabranch
Maximum flow efficiency

ABSTRACT

Arguably, the current planform behaviour of the Indus River is broadly predictable. Between Chashma and Taunsa, Pakistan, the Indus is a 264-km-long multiple-channel reach. Remote sensing imagery, encompassing major floods in 2007 and 2010, shows that the Indus has a minimum of two and a maximum of nine channels, with on average four active channels during the dry season and five during the annual monsoon. Thus, the network structure, if not detailed planform, remains stable even for the record 2010 flood (27,100 $m^3 s^{-1}$; recurrence interval > 100 years). Bankline recession is negligible for discharges less than a peak annual discharge of 6000 $m^3 s^{-1}$ (~80% of mean annual flood). The Maximum Flow Efficiency (MFE) principle demonstrates that the channel network is insensitive to the monsoon floods, which typically peak at 13,200 $m^3 s^{-1}$. Rather, the network is in near-equilibrium with the mean annual flood (7530 $m^3 s^{-1}$). The MFE principle indicates that stable networks have three to four channels, thus the observed stability in the number of active channels accords with the presence of a near-equilibrium reach-scale channel network. Insensitivity to the annual hydrological cycle demonstrates that the timescale for network adjustment is much longer than the timescale of the monsoon hydrograph, with the annual excess water being stored on floodplains rather than being conveyed in an enlarged channel network. The analysis explains the lack of significant channel adjustment following the largest flood in 40 years and the extensive Indus flooding experienced on an annual basis, with its substantial impacts on the populace and agricultural production.

1. Introduction

Changes in the planform of the multiple, divided channel networks that typically characterise the lower courses of the world's largest rivers are conventionally considered unpredictable using approaches developed for smaller rivers (Latrubesse, 2008). However, understanding how such anabranching rivers behave is essential to develop modelling and management schemes for such rivers. The control of water and sediment flux is an urgent issue, as it is linked fundamentally to widespread flooding, infrastructure disruption, population displacement, crop destruction, reservoir sedimentation, and the wider issue of water resources protection more generally (Vita-Finzi, 2012). Huang and Nanson (in a series of papers summarized by Huang and Nanson, 2007, Huang, 2010 and Nanson et al., 2017), appealing to a Maximum Flow Efficiency (MFE) principle, have shown in a mathematical analytical form that a river planform characterised by multiple channels can be the equilibrium and optimal condition for flow that is transporting bedload in a self-adjusting alluvial system. Moreover, this approach allows for a degree of prediction of how the channel patterns will adjust following prescribed changes to the discharge, width and depth, or channel numbers within the system. Such an approach is attractive, not least because it is not overly complex to apply, but such theoretical methods have not yet been tested with robust field data from the world's largest rivers, where the impacts of river adjustment on human populations represent an urgent global challenge. A particular limitation is the need to robustly test such new theoretical approaches to demonstrate the behaviour of channel patterns subject to perturbations to the annual flood pulses that typically characterise the hydrology of large rivers.

* Corresponding author at: Geography and Environment, University of Southampton, Southampton, UK.
E-mail address: P.A.Carling@soton.ac.uk (P.A. Carling).
[1] Present address: Marlborough District Council, 15 Seymour Street, PO Box 443, Blenheim 7240, New Zealand.

https://doi.org/10.1016/j.geomorph.2017.09.021

In this paper, the focus on a multichannel reach of the Indus River in Pakistan is to ascertain if the divided channel pattern has any degree of predictability. The study reach lies downstream of Islamabad, between the Chashma and Taunsa barrages (Fig. 1). Within the study area, the river follows a geological suture and has been in its present location at least since the early Eocene (Clift, 2002). However, the reach has been subject to natural environmental change during the Holocene and to significant human engineering and water abstraction interventions over the last century (Gilmartin, 2015; Syvitski et al., 2013). Despite such potential disruption, this large and powerful alluvial river must be difficult to destabilise, such that it operates today very close to an optimum equilibrium of fluid, sediment, and morphology for prevailing climatic conditions and human interventions at decadal timescales. Whilst local transient states may exist, including lagged adjustments to recent climate change and engineering control, the scale of the system suggests that it is significantly buffered (Dade and Friend, 1998; Clift and Giosan, 2013; Pizzuto et al., 2017) and has evolved iteratively towards an optimum condition to discharge, both fluid and the imposed sediment load, over extended time periods (Dade and Friend, 1998). Even if, owing to a variety of imposed confounding factors such as human impacts, it may not achieve that condition exactly, buffering implies that defining the current near-optimum should be possible. Thus, although such a complex channel network may display elements of stochastic behaviour, it must also exhibit predictable behaviour.

From the arguments above, the aim of this study is to demonstrate that the behaviour of the Indus River study reach is consistent over time and has a degree of predictability in accord with the MFE principle. By corollary, a similar approach might be applied to further understanding of other large rivers. The objectives are to (i) determine channel changes along the study reach through time, inclusive of the impact of a major flood event that occurred in 2010; (ii) test if models of MFE developed using the data from this study could reproduce aspects of the system behaviour; (iii) and to learn lessons about river channel behaviour that might usefully inform river corridor management practices.

Two hypotheses were developed: (1) that channel change through river bank recession is predictable and (2) that the channel network will approach an optimum configuration to transfer the imposed fluid and sediment loads downsystem. From (2) it follows that: (3) the channel network properties should be insensitive to larger, if not exceptional, monsoon-induced flows. This last point is particularly timely given the exceptionally large flood that the Indus experienced during the 2010 monsoon season and in the context that hydrological extremes are likely to become more frequent as a result of likely changes in the hydrology of the Indus River owing to climate change (e.g., Singh and Bengtsson, 2004; Laghari et al., 2012) and future flow regulation (Walton, 2010).

2. The context of the study reach

The study reach is a 264.6-km thalweg-length of the Indus River in Pakistan, with a valley slope (S) of 0.00024 to 0.00028 between the Chashma and Taunsa barrages (Figs. 1 and 2). The annual peak discharge values vary in size, although the timing of the progression of the monsoon flows is consistent (Winston et al., 2013). Annual peak flow occurs between June and late September, during the southwest monsoon. The high flows of the summer monsoon are augmented by snowmelt from the north that transports a large quantity of sediment from the Himalaya southward (Inam et al., 2007). The annual monsoon flood usually peaks at Chashma at discharges of between 5000 and 20,000 $m^3\ s^{-1}$ (Fig. 3), with a mean annual flood (1991–2011) equalling 7530 $m^3\ s^{-1}$ and the 2 year recurrence interval (RI) flood having a discharge of 13,200 $m^3\ s^{-1}$ (Inam et al., 2007), and a 20-year mean annual flow of 3090 $m^3\ s^{-1}$. However, a large flood occurred in 2007 followed by an exceptional flood in 2010 that is the largest recorded since 1929 (Kale, 2014). The 2010 flood is estimated to have peaked at between 27,100 and 29,356 $m^3\ s^{-1}$ (Ali, 2013), with an RI > 100 years. The average daily discharge (1998–2012 data) declines between Chashma and Taunsa by 14%, primarily because of abstraction at Chashma.

Other than basic discharge data, other published information on the Indus River in the study reach is limited (Milliman et al., 1984; Young and Hewitt, 1990; Syvitski and Brackenridge, 2013); so it is worthwhile, at this point, to report an assessment of published data, together with some preliminary data and analyses developed at the inception of this study, to provide context for the Results and Discussion.

The riverbed is alluvial and unconstrained laterally, except where it abuts river terraces or is locally trained by engineering works (Fig. 2). Satellite images show little variability in the meagre natural semiarid vegetation cover and sandy bed material downstream. Individual

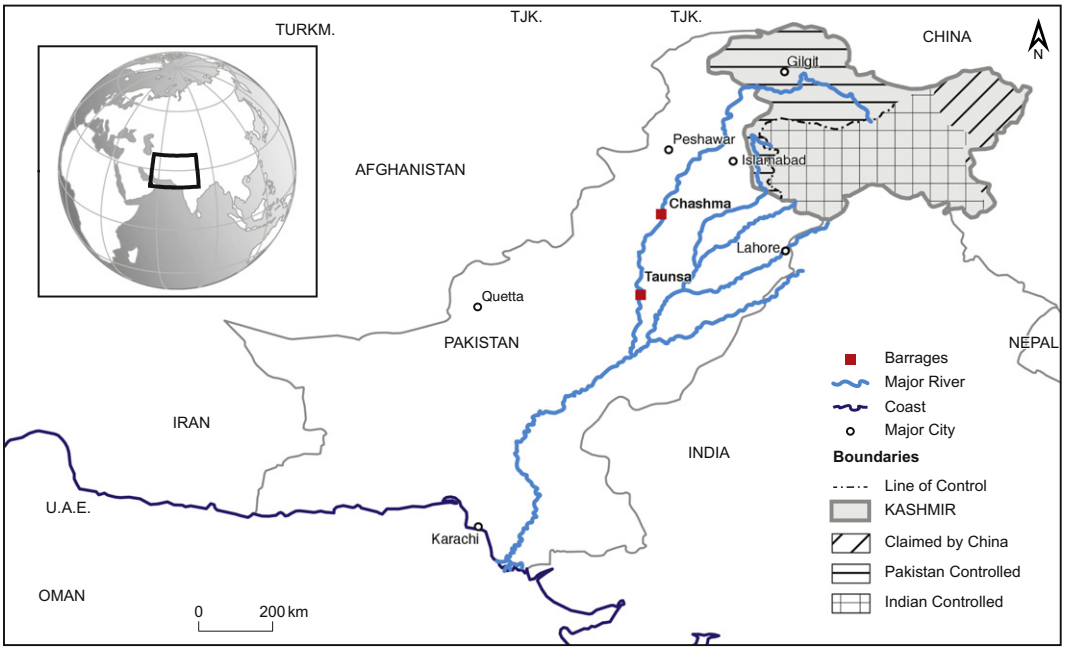

Fig. 1. Location map showing the Indus River and major left bank tributaries within Pakistan.

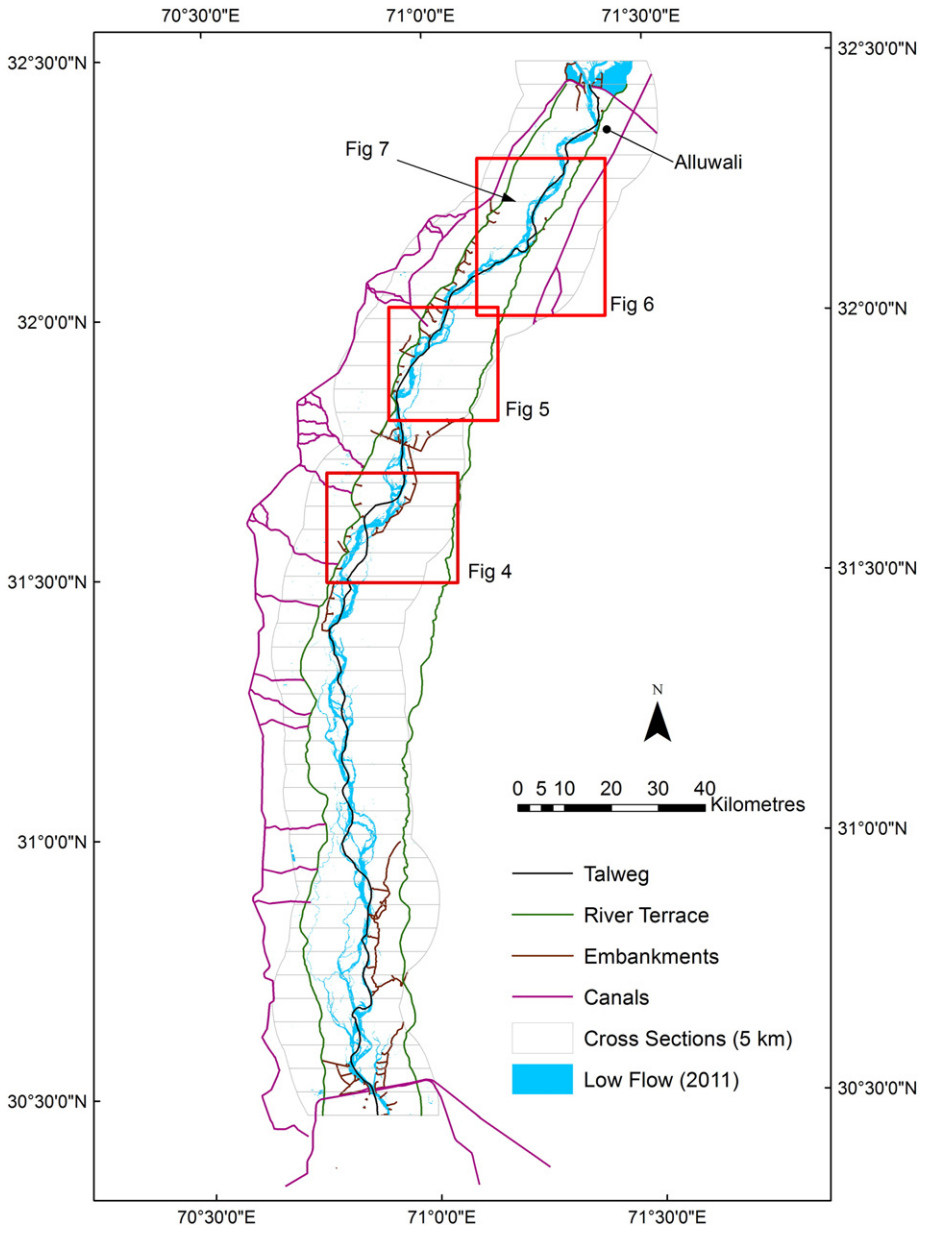

Fig. 2. Schematic image of the study reach. River flow top to bottom. The low flow channel network in 2011 is plotted to illustrate the multichannel nature of the network. The thalweg is defined as the permanently wetted channel identified using all annual data between 1998 and 2011. The Chashma and Taunsa barrages are located at the northern and southern ends of the study reach respectively.

channel widths can range from a few tens of metres to 100 s of metres with some channels up to 6 km wide, including in the dry season when wetted channel widths >1 km remain common. Where the river impinges terraces, the terrace edge (Fig. 2) can be precipitous and up to 25 m above the low water level. The total macrochannel (sensu van Niekerk et al., 1995) is commonly 10 km wide including sand bars, islands, wet channels, and dry channels. The wetted channel planform divides around lightly vegetated, moderately stable islands that are inundated in the monsoon as well as around a multitude of mobile sand bars. In this respect the channel network is considered to be predominately an anastomosed system in accord with the terminology of Carling et al. (2013). Where a single channel dominates, the channel tends to be very wide (~6 km), whereas multithread reaches have narrower channels. There are no published data on channel depths and velocities at high and low flow, so some preliminary field surveys were required that we report at this point (rather than in the Methods and the Results) to provide context for the remainder of the study. No further surveys were possible because of security concerns. Hydraulic field surveys were completed at a section of the main channel near Alluwali (32° 22′ 13.77″ N; 71° 24′ 34.62″ E) immediately downstream of the Chashma barrage (Fig. 2) in September and October 2012. In 2013 the section was surveyed and bank sediment samples obtained. These surveys utilized ADCP and dGPS deployed in a small, powered, rigid boat to monitor velocity, water depth, and channel widths for low flow conditions. Local channel discharges of 1990–4400 $m^3 s^{-1}$ showed that the channel carried around 88% of the flow gauged at Chashma, with the residual discharge passing through four other smaller wetted channels at that section. Surveyed bankfull depths at the cross-sections were between ca. 13 and 19 m. The low flow wetted main channel varied from 741 to 935 m wide, with average water depths ranging between 4 and 9 m. Average flow velocities in these conditions were low, only increasing from 0.93 to 1.24 m s^{-1} over the range of gauged discharges, and Manning's n was constant ~0.08 during these specific surveys. Utilizing local ADCP velocity profiles data, the kinetic streampower Ω was ≤ 7260 W m^{-1}, with a unit streampower $\omega \approx 3.6$ W m^{-2} and bed shear stresses of O 10 N m^{-2}. Estimated flow

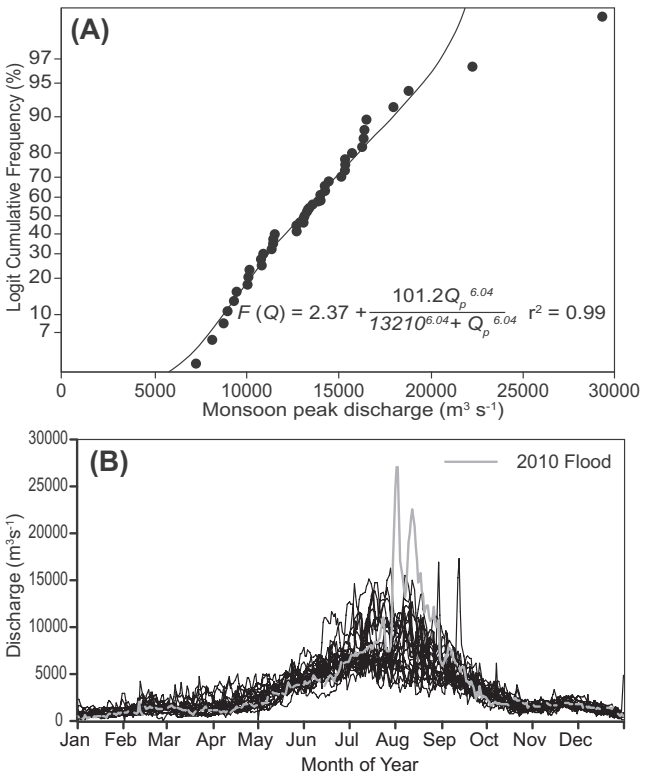

Fig. 3. (A) Distribution of annual peak discharges at Chashma from 1971 to 2012. The high value outlier is the 2010 flood. (B) Comparison of annual hydrographs for 1991 to 2011 (black curves). Note the general similarity of the seasonal trend in the hydrograph shapes and the exceptional peak value for 2010 (grey curve).

depths and bed shear stresses using procedures detailed in Bettess and White (1983) are reasonably consistent with the field data and indicate near-bankfull depths D_b of <13 m and near-bankfull bed shear stresses of *O* 50 N m^{-2}. Similarly, application of the Bettess and White (1983) procedure shows that channel widths increase dramatically as discharge increases, with only a slight increase in depth. The predicted bulk flow velocities increase from 1 m s^{-1} for the mean annual flow in the reach (7530 m^3 s^{-1}) to 2 m s^{-1} for the 2-year recurrent discharge (13,200 m^3 s^{-1}), consistent with the observed low-flow velocities.

Analyses of suspended sediment concentration and suspended load data for the reach are scarce and there are no bedload data (Rehman and Sabir, 1996; Bhatti et al., 2011); but overall the load of the Indus reaching the ocean has reduced since barrages were constructed from the mid-twentieth century (Gupta et al., 2012). Using undefined sediment sampling data from 1902 to 1960, Kirmani (1962) estimated around 366 to 470 metric ton of sediment were delivered to the study reach annually, but he regarded the reach as nonaggrading owing to a comparable efflux downstream. This period of time is before substantial flow controls were constructed on the river, the large Tarbela dam being constructed upstream of the study reach in 1976. The sediment inflow to the Tarbela dam is estimated as 200 metric ton per year, of which around 14% per year is retained in the impoundment (1976 to 2011) (Haq, 2013). This sediment retention has resulted in the load at Chashma now being estimated as around 75 metric ton per year and 84 metric ton per year at Taunsa (Haq, 2013). Despite the apparent increase in load downstream, aggradation is occurring upstream of Taunsa (Gaurav et al., 2011). According to Kirmani (1962) around 88% of the total load is transported during the monsoon season, and suspended sediment concentrations at that time are within the range 120 to 180 mg L^{-1}. These various determinations of suspended load should be treated with caution (concentrations seem low - *vis* Sabir et al., 2013 - and may reflect near-surface sampling Rehman and Sabir, 1996) but provide an order of magnitude estimate of the minimum suspended sediment load in the study reach. Dade and Friend (1998) reported the bed grain size as sand (d_{50} = 0.18 mm) and a Rouse number w_s/u_* of 0.31 for low (where w_s is the settling velocity and u_* is the shear velocity). Based on these meagre data, we can anticipate that much of the bed sediment would be in suspension at low flows, although Kirmani (1962) reported 'clear-water' flows in the dry season. The bank top sediments are fine, noncohesive sediment (d_{50} = 0.049 mm) and thus are readily erodible.

3. Method

3.1. Remote sensing

Landsat 5/7TM data (resolution 30 m) were obtained from the USGS website (http://earthexplorer.usgs.gov/) and supplemented by SPOT images (resolution 20 m) supplied by the Space and Upper Atmosphere Research Commission (SUPARCO) of Pakistan (Table 1). Tiles free of substantial cloud cover were processed for the high flow and low flow periods of each year from 1998 to 2012. No high flow Landsat data were available for 2003. Images were acquired within the UTM 42 N zone projection that references the WGS84 datum and no atmospheric correction was required (Song et al., 2001). A 15-km-wide buffer polygon was segmented into 5-km subreaches (Fig. 2); the latter used for collating channel change data at fixed downstream sampling intervals. The choice of 5-km spacings for cross sections is based on the axiom that sections spaced at intervals equal to between 3 and 10 channel widths are required to represent channel morphology adequately (e.g., Yalin, 1977; Samuels, 1990; Miori et al., 2006). As the major wetted channels are at least 1 km wide, the 5-km spacing seems appropriate. This supposition was tested in a post hoc analysis using time-series analysis techniques (Hamilton, 1994; Chatfield, 1996) as is explained further in the Results.

To enable statistics to be collected for left and right bank, a river macrochannel centreline following the thalweg was determined and used to split the subreaches into left or right bank elements. Landsat and SPOT images were converted into raster data sets reclassifying the image into three categories: water, bare ground and vegetated ground (Fig. 4) for the low flow periods, year-by-year, using unsupervised classification for Landsat and supervised classification for SPOT images; the latter resampled to 30 m resolution for comparability with Landsat imagery. Bare ground consisted primarily of channel sand bars, floodplain sand splays, and some floodplain scour holes. Thus, losses in any type of vegetated land (comparing sequent low flow periods) were regarded as areas of land lost owing to the intervening monsoon flood peak flow.

3.2. Time-series analysis

In order to determine if the 5-km spacing of sampling cross sections noted in the above section are representative of reach-scale processes, time-series analysis techniques (Hamilton, 1994; Chatfield, 1996) were applied to the bank erosion data, treating the cross sections as a downstream spatial series.

For brevity this method is not explained here but is presented by Meshkova and Carling (2013). Autocorrelation (ACF) and partial autocorrelation (PACF) functions for the data series were obtained using MiniTab 16 (MiniTab Inc.) software. Autocorrelation analysis in this application describes the correlation of each single data point in a spatial series with its neighbouring upstream or downstream values, such that the analysis provides some indication of 'memory' in the data series along the channel. Thus, it is useful to determine more precisely the significant lag value beyond which there is no statistical persistence (i.e., no 'memory' between a given data point and data

Table 1
Availability of Landsat and SPOT satellite data in relation to the variation in river discharge at the Chashma barrage.

Year	Satellite	Sensor	Resolution (m)[a]	High flow Period	Low flow Period[b]	HF period Discharge ($m^3 s^{-1}$)	LF period Discharge ($m^3 s^{-1}$)
1998	Landsat 5	TM	30	8/27/98	5/23/98	6467	5658
1999	Landsat 5 and 7	ETM + and TM	30	8/6/99	2/19/99	12,244	1727
2000	Landsat 5	ETM + and TM	30	8/8/00	2/22/00	4531	1218
2001	Landsat 5	ETM + and TM	30	8/27/01	3/4/01	5510	622
2002	Landsat 7	ETM +	30	7/29/02	2/19/02 and 4/23/02	4201	663
							1524
2003	Landsat 7	ETM +	30	N/A	3/10/03		1359
2005	SPOT 4	HRVIR	20	10/11/05	3/24/05 and 3/28/05	1614	2422
							1617
2006	SPOT 4	HRVIR	20	9/30/06	1/02/06, 1/07/06	2917	425
							510
2008	SPOT 4	HRVIR	20	8/26/08	1/02/08, 3/25/08 and 3/29/08	4247	311
							679
							616
2009	LANDSAT 5	TM	30	7/08/09	5/21/09	5154	3681
2010	LANDSAT 5	TM	30	6/09/10	5/24/10	4729	3540
2011	LANDSAT 5	TM	30	10/02/11	3/24/11	2174	1133
2012	SPOT 4	HRVIR	20	9/18/12	1/24/12, 1/29/12 and 2/03/12	5318	849
							849
							1246

[a] SPOT imagery was originally supplied as 20 m resolution data but this was resampled to 30 m prior to land loss analysis.
[b] For low flow periods, in some years it was not possible to cover the study area with imagery taken for a single date, thus these periods are a composite of days.

values at a given lag upstream or downstream). For example, once the correlation between individual cross sections at given lags falls below a selected confidence limit (in this paper 95% is used), the data points can be considered uncorrelated. Thus, if the cross sections are spaced at 5 km and the correlation becomes nonsignificant at lag 3, it might be interpreted that there is no downstream memory in the series after a distance of 15 km.

3.3. Selection of representative discharge

In all analyses below, the discharge quoted is from the Chashma barrage downstream gauge. A positive relationship can be reasonably expected between the area of vegetated land lost and some measure of the monsoon peak flow. However, low flows will result in negligible land loss, so there likely is a threshold discharge value (Q_c) below which

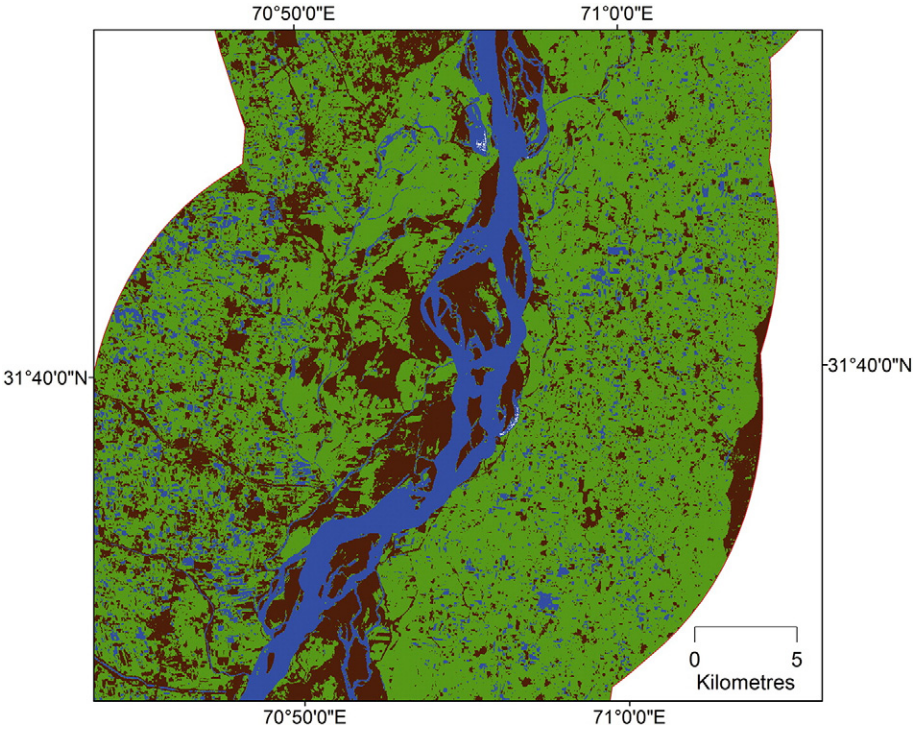

Fig. 4. Example of processed data for dry season low flow during 2011 discharge is 1133 $m^3 s^{-1}$. Green is vegetated land; brown is bare ground; blue is open water. Flow top to bottom. The location of this reach is shown in Fig. 2.

significant land loss does not occur, bank retreat is minor, and changes to the channel network are unlikely. In similar fashion, there should be a relationship between discharges flooding overbank and the area flooded. There is a general understanding that bank erosion is a positive function of discharge (e.g., Gares et al., 1994). For example, Darby et al. (2010) used an excess shear stress function to describe bank recession rates (ε) that reduces to a linear or power function of discharge depending on local site characteristics. To explore the relationship between discharge and annual land loss a representative annual discharge is required. Peak discharge Q_p clearly is a simple and convenient index of the applied streampower associated with the annual flood hydrograph (Magilligan et al., 2015). As bank erosion generally does not occur for low flows, sometimes it is advocated to integrate the discharge or the streampower above a given threshold Q_c throughout a flood as a measure of the energy available for bank erosion (e.g., Costa and O'Connor, 1995; Sear, 2004; Darby et al., 2010). Thus, considering only $Q_p - Q_c$, rather than integrating above a threshold, river bank recession (or land lost) might conveniently be indexed by the function.

$$\varepsilon = k(Q_p - Q_c) + a \tag{1}$$

where the bank erodibility coefficient k and the regression constant a are determined empirically. A benefit of considering a monsoon system is that, in the main, the hydrograph is a simple single-peak event with a large peak value in contrast to the discharge values in the low flow period (Fig. 3B). Preliminary calculations (not reported herein) showed that use of the annual peak discharge value provided just as good an empirical index of the annual flood's ability to induce land loss as consideration of an integrated discharge above a threshold or consideration of integrated power. Consequently, peak discharge values are used herein, as these values are more useful for routine application to risk assessment (Khan et al., 2011).

3.4. Equilibrium channel network

Crosato and Mosselman (2009), Huang and Nanson (2007), Eaton et al. (2010), and Nicholas (2013a, 2013b) have determined from theory that stable channel networks have few channels. Stability is defined herein as a network having the same number of channels through time and space. Eaton et al. (2010, p. 356) stated that 'stable anabranch channels exhibit two or possibly three channel threads, but not more'; whereas Huang and Nanson (2007) argued for three to four channels as being stable. The key observation, in both cases, is the small number of channels that theoretically constitute a stable channel network (Bolla Pittaluga et al., 2003; Kleinhans et al., 2008).

Here we apply the concept of Maximum Flow Efficiency (MFE) as defined by Huang and Nanson (2007). Minor typographic errors that occurred in some of the equations published by Huang and Nanson (2007) are corrected as given below. Huang and Nanson (2007) demonstrated that in low gradient systems, where gradients cannot be increased, multiple-channel networks are more efficient for sediment transport than single channels. These rivers must evolve to achieve MFE, whereby the maximum amount of sediment is transported per unit of applied stream power within the given number of channels. The theory is expounded in Huang and Nanson (2007, and earlier work cited therein) and for brevity the derivations of key equations are not provided here as they have been provided prior (Huang and Nanson, 2007). Huang and Nanson (2007) made use of the revised Meyer-Peter and Müller (1948) bedload transport function as developed by Wong and Parker (2006). Fundamentally, for a given discharge Q, slope S and bed grain size d, a teleological adjustment to channel form (indexed by $W/D = \zeta$, and η the number of channels) follows such that the bedload sediment transport approaches a maximized aggregate value across all channels.

The bedload sediment discharge for the total of channel widths is

$$Q_s = K_1 \zeta^{3/8} (\zeta + 2)^{1/4} \left[K_2 \frac{\zeta^{3/8}}{(\zeta + 2)^{\frac{3}{4}}} - K_3 \right]^{1.6} \tag{2}$$

where ζ is the width/depth ratio and K_1, K_2, and K_3 are coefficients calculated as below:

$$\zeta = \frac{W}{D}$$

$$K_1 = 4.93 \sqrt{\left(\frac{\rho_s}{\rho} - 1\right) g} d^{25/16} \left(\frac{Q}{7.68\sqrt{gS}} \right)^{3/8}$$

$$K_2 = \frac{S^{13/16}}{\left(\frac{\rho_s}{\rho} - 1\right) d^{15/16}} \left(\frac{Q}{7.68\sqrt{gS}} \right)^{3/8}$$

$$K_3 = 0.0470$$

For multiple channels, the coefficients K_1 and K_2 are redefined as

$$K_1 = 4.93 \eta^{5/8} \sqrt{\left(\frac{\rho_s}{\rho} - 1\right) g} d^{25/16} \left(\frac{Q}{7.68\sqrt{gS}} \right)^{3/8}$$

$$K_2 = \frac{S^{13/16}}{\left(\frac{\rho_s}{\rho} - 1\right) d^{15/16}} \left(\frac{Q/\eta}{7.68\sqrt{gS}} \right)^{3/8}$$

where η introduces the effect of the number of channels.

In an alluvial channel with a given width, channel depth is the only geometric variable that is fully adjustable, which is a useful outcome in the case of the Indus where channel depths are ill-defined. The bedload sediment discharge is then obtained as:

$$Q_s = K_1 \left[K_2 D^{-3/2} - K_3 \right]^{1.6} \tag{3}$$

where K_1 and K_2 are defined as

$$K_1 = 4.93 W \eta \sqrt{\left(\frac{\rho_s}{\rho} - 1\right) g d^3}$$

$$K_2 = \frac{S^{1/4}}{\left(\frac{\rho_s}{\rho} - 1\right) d^{3/4}} \left(\frac{Q/\eta}{7.68 W \sqrt{g}} \right)^{3/2}$$

For a given channel width, the river depth D is determined using a trial-and-error method:

$$D^{5/2} = \left(\frac{d^{1/6} Q}{7.68\sqrt{gS}} \right)^{3/2} \frac{(W_t + 2\eta D)}{W_t^{5/2}} \tag{4}$$

where $W_t = W\eta$.

The test cross section chosen in the Indus was the section at Alluwali (see Fig. 2) detailed in Section 2, as this is the only section for which there are sufficient hydraulic and geometric data available. As well as applying Eqs. (2) and (3) above, the effect of partitioning the discharge between channels was also examined. In the absence of other information, the discharges gauged at Chashma on each of the days of the field surveys were proportioned between channels in direct relationship to their widths. This procedure resulted in 62% of the flow being assigned

to the widest channel, whereas the field survey indicated 88% was the appropriate discharge. The difference reflects the unknown depth factor, so the issue of unknown depth was considered further. Iterative application of Eq. (4), commencing with an estimated water depth, for each of the five measured channel widths resulted in little difference in predicted channel depths ~2.5 m. Note that this value is on the low side of the observed depths noted during the field surveys of the main channel and may reflect very shallow flows in the subsidiary channels. Nevertheless, bedload sediment discharge within each channel also was calculated using the Huang and Nanson (2007) model as well as being calculated for the sum of the five channel widths as if one wide channel existed. Because of the minimal difference in calculated depths the difference in the estimated bedload was only 0.14%. Calculations using Eqs. (2) and (3) were made to determine the maximum bedload sediment transport rate Q_s, ς, and η for a typical annual monsoon peak flow (7530 $m^3\ s^{-1}$), the 2-year RI (13,000 $m^3\ s^{-1}$), and for the record flood of 2010 (27,100 $m^3\ s^{-1}$).

4. Results

4.1. General observations

In this section some general observations are made that were derived from the extensive analysis of the remote sensing data. In the following sections (4.2 and 4.3), network adjustment is considered more fully and quantitatively.

The expansion of the wetted area from low flow to high flow rarely includes development of new channels. Rather, dry channels are reoccupied annually, as is evident in Fig. 5. In Fig. 6A it may be seen that some low flow channels are always occupied, whereas others are occupied intermittently. It is evident that high occupancy occurs close to a centrally located thalweg with lower and variable occupancy either side of the thalweg. This lateral decline and variable occupancy can only occur because of lateral erosion of the margins of the macrochannel in some years, with concomitant sedimentation on the opposing macrochannel margin (see Section 4.2). Note, however, that the low flow network pattern is consistent year after year, occupying a relatively constrained corridor, albeit with some lateral expansion in a few years. A degree of low flow network stability, if not individual channel stability, is evident. Fig. 6B depicts the low flow channel pattern the year after the 2010 flood. Although, as shown in Fig. 6C, some channel change was evident by 2012, there is an overriding tendency to repeat the high flow channel pattern year after year; although year by year, different channels may have greater or less dominance in terms of discharge. Thus, rather than extensive change in the network geometry, the 2010 flood primarily resulted in the formation of new sand bars, as picked out in Fig. 6C, river banks retreated (as described in the following section), and extensive deposition of sediment occurred across the floodplain.

Vegetated river bank retreat occurs primarily at outer bank locations of low radius, high curvature bends. An example of this association is presented in Fig. 7. In this example, bend extension, resulting in the loss of vegetated land, has occurred at the point of tightest channel curvature on the true right bank by vegetated land converting to open water (effectively river bank erosion), with an associated loss of productive agricultural land. At the same time, much of the wetted area on the left bank has converted to bare sand bars. Nevertheless, increase in curvature has resulted in an incipient cutoff channel developing across a stabilizing point bar where vegetation is colonizing bare sand.

From the above (Figs. 5 through 7) the macrochannel behaviour, in terms of the number of channels, is clearly shown to be quite stable year after year. Fig. 8 shows the number of wetted channels observed for the Chashma-Taunsa reach for each year from 1998 to 2012, at low flow and high flow conditions. The channels are counted from 44 subreaches of 5 km length. As well as having a well-defined low flow thalweg (Fig. 6A), the Indus is characterized by a minimum of two and a maximum of nine channels in total for any given surveyed cross section. The average number for the low flow season is 4.7 with a standard deviation of 1.6, while in the high flow season the number

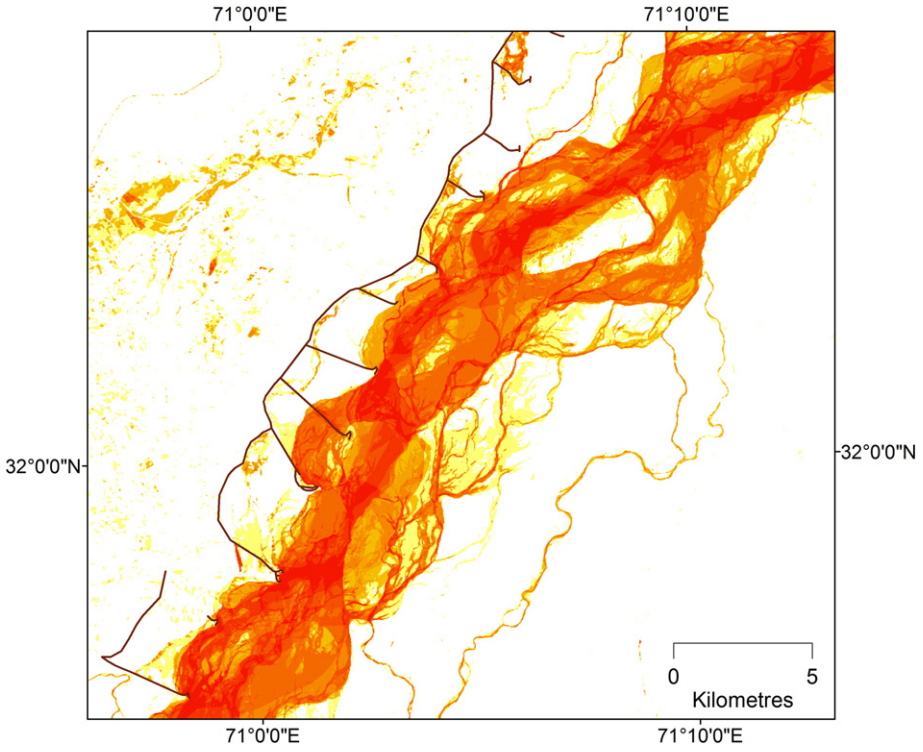

Fig. 5. Expansion of the wetted area over nine flood seasons during the high flow period. The darkest red represents locations wetted in all nine years and thus the persistent wetted channel network; brown shading represents less frequent channel locations, whilst yellow represents high flow inundation (including west-bank major canals). White areas were never flooded. Flow top to bottom. The location of this reach is shown in Fig. 2.

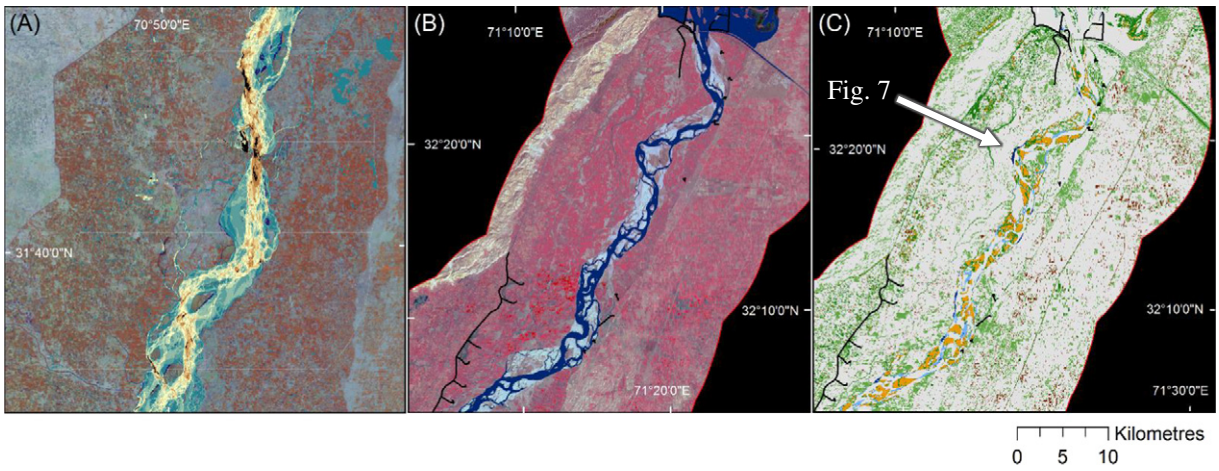

Fig. 6. (A) Low flow wetted channels superimposed for 9 years of data obtained for the period 1998 to 2011. Dark red hue is floodplain. Within the macrochannel the darkest hue indicates the channel was wet in all nine years, whilst progressively lighter hues indicate less frequent wetting with white indicating wetting in only one year of the nine, (B) Low flow wetted channels in 2012, (C) Low flow image of the river system early in 2012. Blue represents vegetated areas (in 2011) changing to open water; Dark green represents water changing to vegetation; light green represents bare areas changing to vegetation; yellow represents wetted areas changing to new sand bars; white represents agricultural land; dark red indicates settlements; dense black lines are river training works. Flow top to bottom in all panels. The location of this reach is shown in Fig. 2.

of channels is higher with an average of 5.6 and a standard deviation of 2.1. Overall, the high flow season has one more channel than the low flow season. On average, ignoring seasonal variation and spatial change, the number of channels observed in this study reach is five, but about four channels are wet during the dry season and five during the monsoon.

4.2. River bank recession

Hypotheses (1) is tested within this section.

In Fig. 9 it is evident that the vegetated land loss following the 2010 flood was equal to or up to four times as great as the land loss related to lesser monsoon floods in the previous 10 years. However, this loss was primarily owing to conversion of vegetated areas, including agriculture, to bare sand rather than to wetted channel network expansion. Thus, we may infer that the exceptional flood of 2010 deposited sand extensively because of the prolonged deep-inundation of the floodplain. Conversion of vegetation to bare ground would also have been greater in 2010 owing to the long period of deep inundation, that would lead to vegetation die-back which will be less prevalent when the duration and depth of inundation (because of lower level floods) is less. Consequently, the duration of inundation is also a likely factor in the expansion of sandy areas and in the potential destabilization of the network related to loss of riparian vegetation. Land losses were fairly evenly distributed throughout the study reach (Fig. 10).

Thus, to consider channel change more specifically, it is necessary to concentrate on the loss of riparian land on the right and left banks down the full length of the system. The land lost each year relative to the peak discharge was determined for right and left banks at each of 44 5-km spaced cross-sections, yielding 88 determinations, as illustrated for a single cross section in Fig. 11. Despite the inevitable bunching of data for discharges up to 15,000 $m^3 s^{-1}$ and in contrast to the plotted position

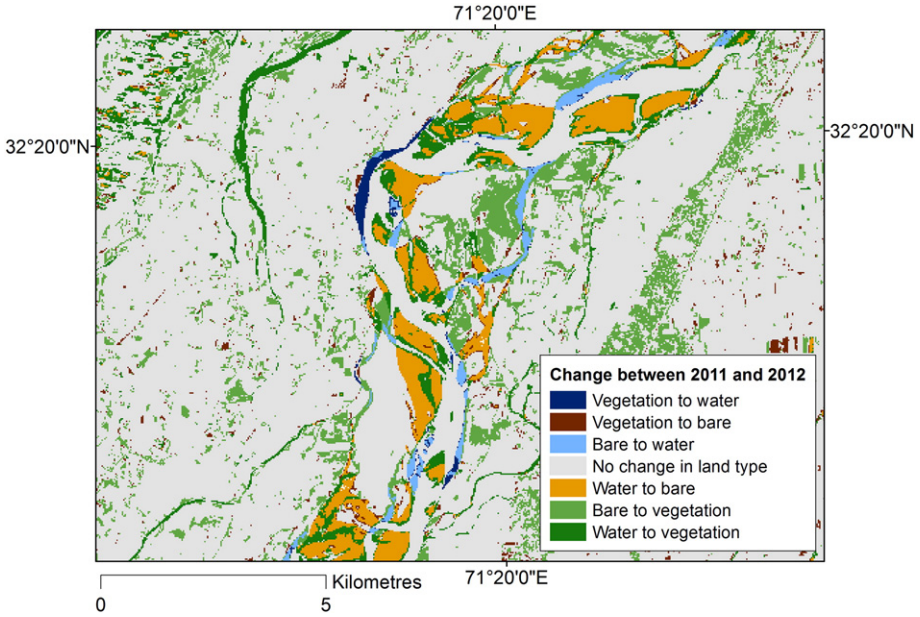

Fig. 7. A zoomed view of a channel bend shown in Fig. 6C showing the detail of bend extension over one year. The location of this reach is shown in Figs. 2 and 6C. In this reach there is a clear association between apex of the channel bends and the loss of vegetation (vegetation to water). There is also considerable loss of vegetation throughout the distributive channels.

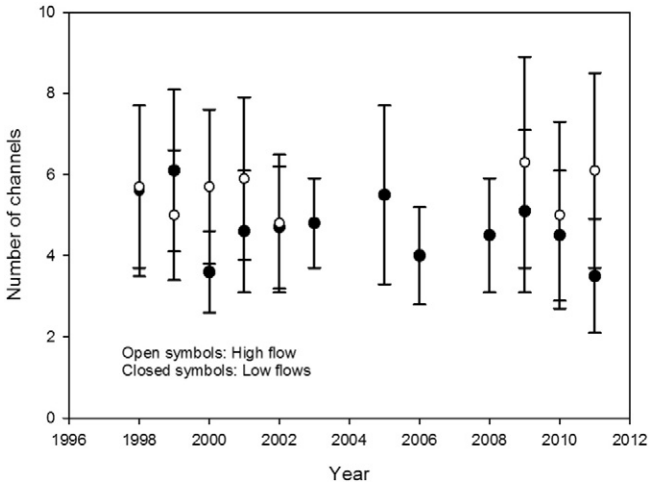

Fig. 8. Number of channels observed in low flow and high flow season from 1998 to 2012.

of the 2010 datum, a number of signal points arise. Considering all sections, 70% exhibited positive linear relationships (Eq. 1) with 53% of these examples being statistically significant ($P < 0.05$, $r^2 > 0.36$, $N > 9$). Thirty percent of sections had weak, nonsignificant ($P > 0.05$) negative or indeterminate relationships. Some 62% of positive relationships trended towards an intercept of zero land loss around a discharge value of 6000 $m^3\ s^{-1}$, which value can be considered as the bank erosion threshold value Q_c. Consequently, all positive regressions were constrained to intercept the *x*-axis where $Q = 6000\ m^3\ s^{-1}$. Ninety-five percent confidence limits around zero-intercept regression curves demonstrated that the true intercept could lie between 0 and 13,000 $m^3\ s^{-1}$ (not illustrated). As the monsoon flood rarely peaks below 6000 $m^3\ s^{-1}$, it is possible to discount intercept values $<6000\ m^3\ s^{-1}$. In addition, as six of the study years exhibited land lost for peak discharges $<13{,}000\ m^3\ s^{-1}$, it is not unreasonable to accept a threshold Q_c value of 6000 $m^3\ s^{-1}$ for practical applications.

For each section with significant trends, hindcasts and forecasts are possible, as shown in Fig. 11. Because there is a significant end-point control imposed on the slope of all positive regression lines by the 2010 datum at 27,100 $m^3\ s^{-1}$, 95% confidence limits and standard error ranges were fitted to all cases to determine the uncertainty in land loss. In this manner, the uncertainty in likely land lost can be explored for any given discharge. For example, in Fig. 11 the uncertainty of predicted land lost using the plotted curve is shown by standard error bars. To test the applicability of such an approach, supplementary land loss data (derived from satellite imagery) for seven additional years also are plotted (2003 to 2008 and 2011). These data were not available at the time of the main analysis, but importantly these points were not included in deriving the regression equation. Three of the observations fall within the range of the associated uncertainty, giving some confidence in the general approach. It is not clear however if the apparent linearity of bank erosion as a function of peak discharge represents the true process response. For example, for very large overbank floods one might anticipate that bank erosion might reduce, owing to much water being transferred downsystem over the floodplain, away from banklines. In contrast, bank erosion might increase for very high floods related to the increased power applied to the banks especially during falling flows as the energy gradient of water running off the floodplains steepen as banks emerge. Additional data for high-flow years would be required to test this point.

Comment is necessary with respect to the negative or indeterminate regressions that represent 30% of the sample. In most cases the coefficients of determination (r^2) were low and not significant. Using remote sensing it is easier to identify a clean-cut bankline in contrast to the margin of an accreting sandy point bar. The former should have well-defined interfaces between vegetated land and water, whilst the latter will have ill-defined interfaces because of shallow water on low-angle sand bars and a lack of riparian vegetation. Nevertheless, negative regressions can be ascribed to some degree of lateral accumulation into a channel that was previously wetted. Notwithstanding, it is clear then that, with 70% of regressions being positive, the macrochannel tends to widen on high flows and widened appreciably in 2010, without defined compensating lateral accretion during the same event. In this

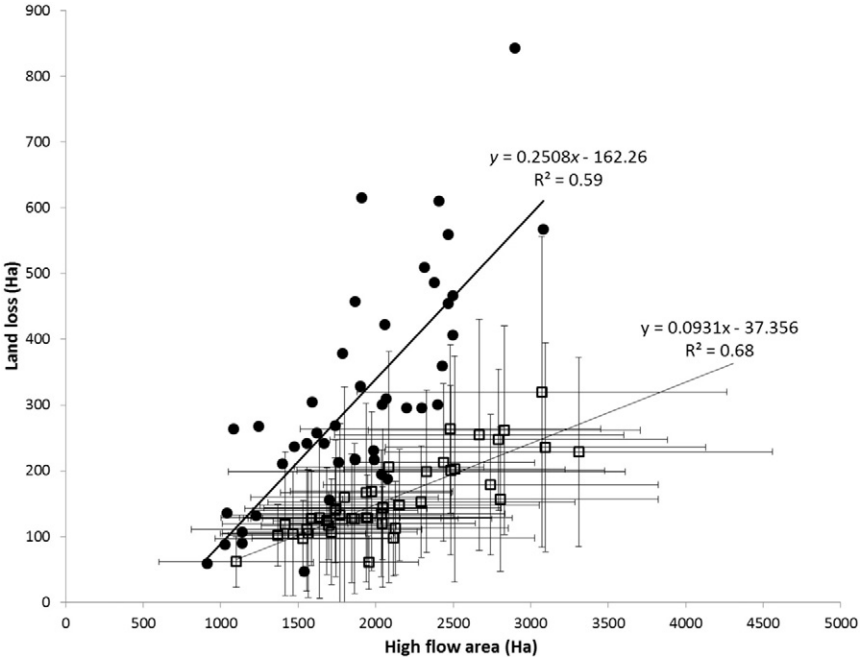

Fig. 9. Comparison of the area flooded during annual floods and the amount of vegetated land lost each year. Square symbols represent average values per 5-km reach on the left and right banks for typical monsoon flood conditions (1998–2009). Error bars represent variation across 47 5 km-spaced cross sections over the 240-km reach. Dots represent the disproportionate land losses owing to the flood of 2010.

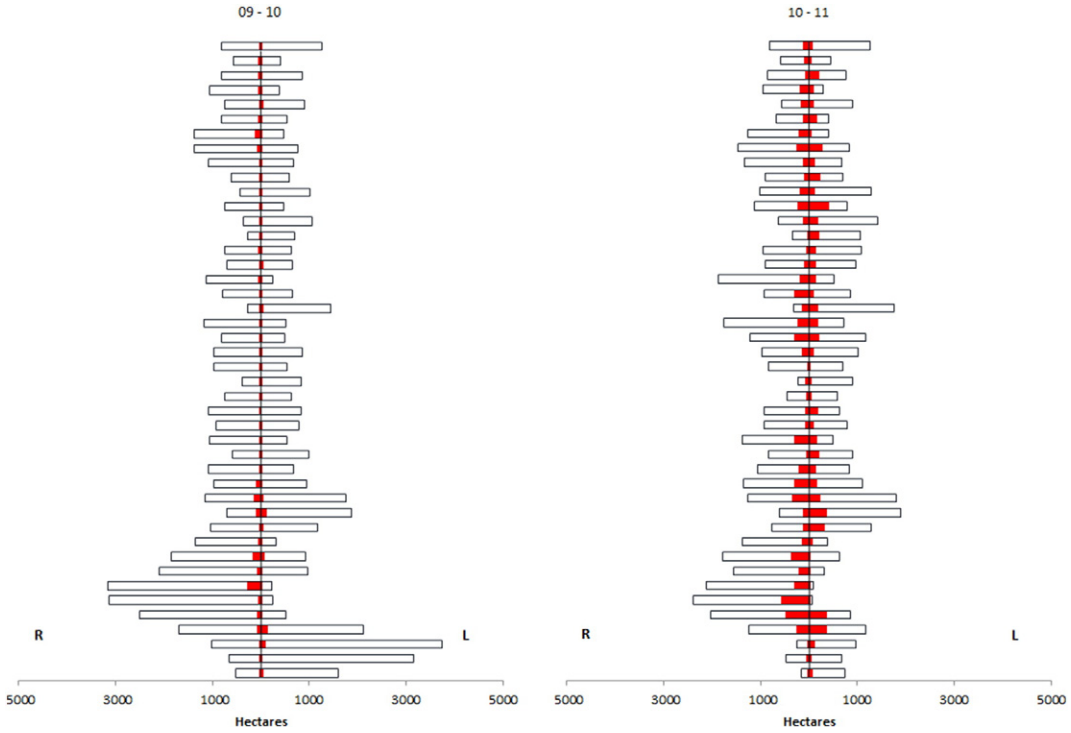

Fig. 10. Schematic comparing vegetated land lost (ha) on the right (R) and left (L) banks of the Indus following the monsoon flood of 2009, as recorded in 2010, and in 2010–2011. Base of the chart is to the south. White bars are the areas of the high flow mask for the left/right bank used to identify land change each year. Red bars are the areas of previously vegetated land that became water or bare sand. There are 52 5-km rows in the grid but rows 1–3 and 48 + are excluded from analysis as they occur upstream and downstream of the barrages.

manner, it appears that the system capacity expands as discharge increases. This conclusion is in accord with the more general interpretation of Figs. 6C, 7, and 9.

Reviewing the positive (erosion) or negative (aggradation) sign of the regression relationships, it was evident that there was some grouping of signs for sections in a downstream direction with several tens of kilometres being dominated by either positive or negative signs (Fig. 12) that might reflect reach-scale changes in river behaviour. Alluvial rivers tend to incise and narrow when the ratio of sediment supply to transport capacity decreases, and they tend to aggrade and broaden when that ratio increases (e.g., Bull, 1991). The predominance of channel widening by erosion immediately downstream of the Chashma barrage (completed 1971) and deposition upstream of the Taunsa barrage (completed 1958) is as might be expected and as observed prior (Gaurav et al., 2011), with bed degradation below barrages (Kondolf, 1997) and aggradation above them being a common response (Evans et al., 2007). The controls on the variability observed in the middle reaches are yet to be investigated. The extents of the downstream impact of the Chashma barrage (ca. 30 km of channel widening) and the upstream impact of the Taunsa barrage (15 to 45 km of channel narrowing: see Discussion) on land lost or gained provide some indication of the maximum timescales associated with significant channel change. Adopting 2010 as the baseline date for this study, the Chashma barrage has induced changes within 39 years, whilst for the Taunsa barrage changes are within 57 years. Thus, measurable channel changes occurred over many kilometres within only several decades.

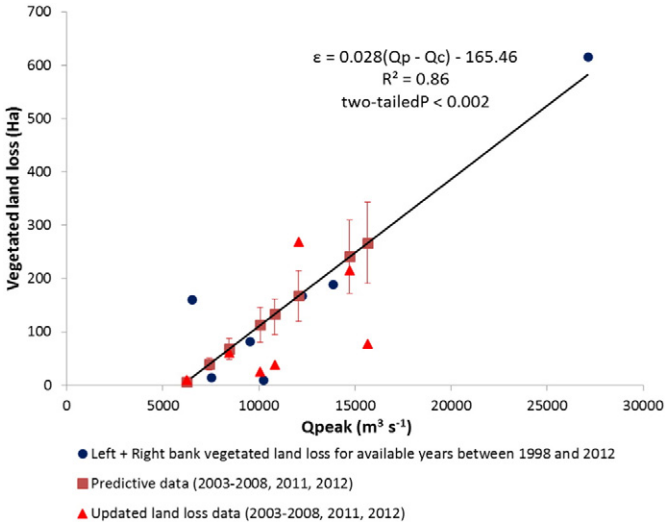

Fig. 11. Example of land lost at cross-section 36. Land was lost on both banks so the data for both banks are summed ($N = 7$). The standard error bars provide discharge specific estimates of uncertainty in predicted land loss.

The time-series analysis demonstrated nonrandom section behaviour (not illustrated). Autocorrelation and partial autocorrelation between sections indicate >60% probability that the result at any one section is applicable to the next neighbour (10 km reach) and possibly 20-km reach. Although a higher percentage probability would be preferable to transfer inferences derived at 5-km-spaced sections to intermediate locations, it is otherwise remarkable that a multichannel network that initially appears somewhat chaotic, or at least stochastic, in planform behaviour should exhibit spatial 'memory' along reaches measured in tens of kilometres.

Consequently, hypothesis (1), that channel change through river bank recession is predictable, is supported by the analyses above.

4.3. Channel network stability

Hypotheses (2) is tested within this section.

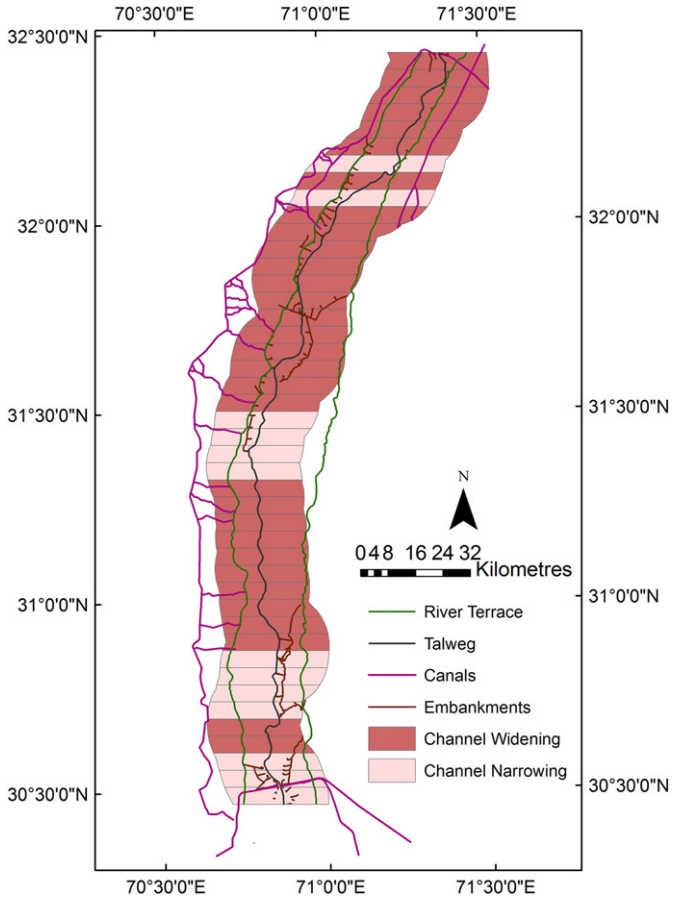

Fig. 12. Zonation of widening and narrowing subreaches within the 264.6-km study reach. River flow top to bottom. The Chashma and Taunsa barrages are located at the northern and southern ends of the study reach respectively.

The model of Huang and Nanson (2007) is applied to the Indus River for the example of cross section 23 at Alluwali. Analysis considered (i) the optimal sediment transport for an hypothetical single channel with an aggregate width-depth ratio ς for the five channels observed at this section that conveys the gauged discharge (Fig. 13A), and (ii) for five individual channels ($\eta = 5$ is the average observed from 1998 to 2012; Figs. 8 and 13B). As detailed by Huang and Nanson (2007), the sediment discharge function has a dome shape, with the peak value of the maximum sediment transport capacity located at the optimum ς value. In the case of the Indus River and for the average monsoon peak flow of 7530 $m^3 s^{-1}$, the optimum ς ratio for one aggregate channel is 2650 with the maximum Qs value of 0.1787 $m^3 s^{-1}$. The optimal ς value for a 7530 $m^3 s^{-1}$ flood may be compared with the low flow field data where D was O 1–9 m, channel aggregate width was 2720 m and observed aggregate ς values varied from ca. 600 to 2720 as discharge varied. These results imply that the system should become more efficient during high flows when the wetted widths increase substantially in contrast to depth increases of only several metres.

Solution of Eqs. (2) and (3) for a very small discharge (3000 $m^3 s^{-1}$) produced vanishingly small bedload sediment transport rates, which is consistent with the argument given above that a threshold for river bank erosion lies around a monsoon peak discharge value of 6000 $m^3 s^{-1}$. Increasing the peak discharge to 13,200 $m^3 s^{-1}$ (2-year RI flood) and then to 27,100 $m^3 s^{-1}$ (record 2010 flood) caused the optimal value of ς to increase somewhat as the maximum sediment transport rate increased from 0.3087 to 0.6435 $m^3 s^{-1}$. The peak in the dome-shaped sediment discharge curve became flatter and broader, such that the optimum value of ς was not achieved so readily for the range of parameter values. In the same manner, increasing the number of channels from 1 to 5 resulted in a small but consistent reduction in bedload sediment transport rate. Taken together, it is evident that for the range of parameter values that reasonably apply to the Indus, the optimum in bedload transport rate is most readily achieved for a peak discharge in the vicinity of 7530 $m^3 s^{-1}$ with a reasonable result obtained for 13,000 $m^3 s^{-1}$ and progressively less acceptable solutions as peak discharge rises further.

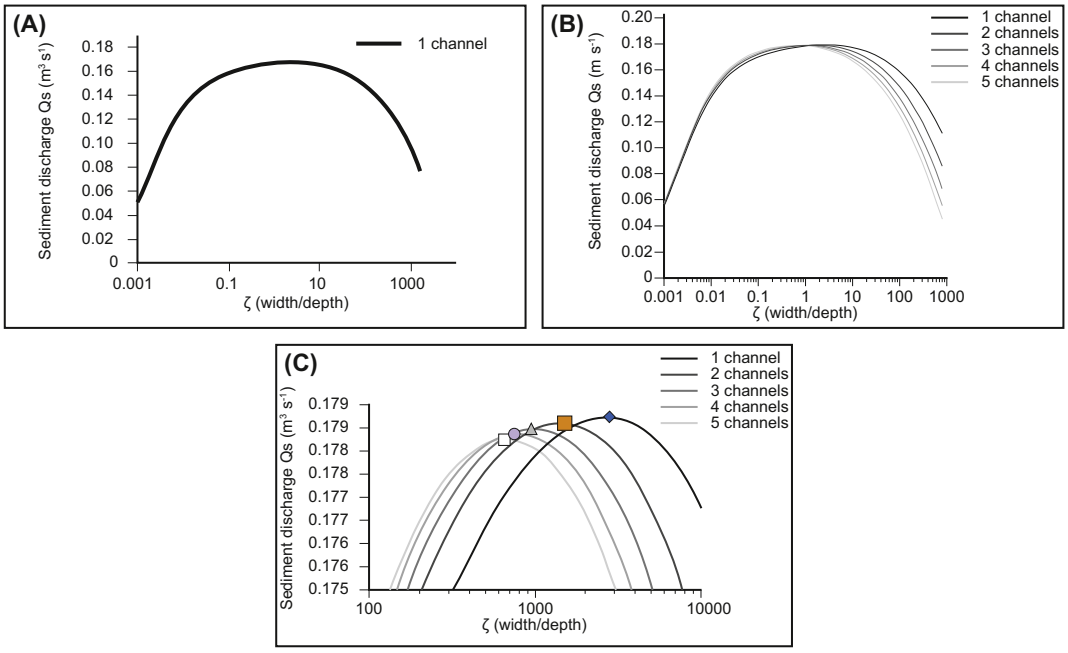

Fig. 13. Sediment discharge Qs vs. the width/depth ratio ς for (A) a single channel of aggregate width equal to all five channels; (B) variation of sediment discharge Qs versus ς of each individual channel for $\eta = 1$ to 5; (C) zoomed view of the apices of the curves in B. $Q = 7530$ $m^3 s^{-1}$, $S = 0.00028$, and $d_{50} = 0.18$ mm in all panels. Symbols show locations of apices of each curve.

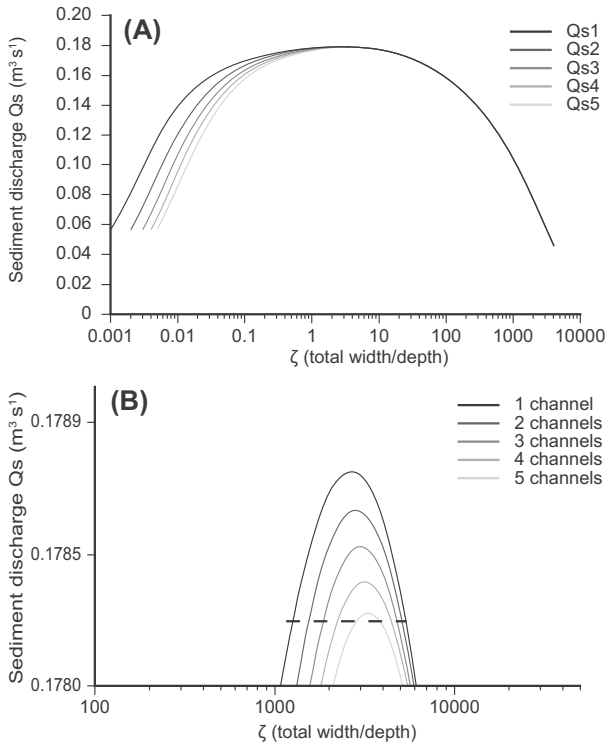

Fig. 14. (A) Variation of sediment discharge *Qs* vs. ς of the whole anabranching system against the number of channels η; (B) zoomed view of the apices of the curves in panel A; $Q = 7530\ m^3\ s^{-1}$, $S = 0.00028$, and $d_{50} = 0.18$ mm in all panels.

In the five-channel system of the Indus River (Fig. 13B), it is hard to see peak sediment transport because of the broad shape of the peaks to the curves, so a close up view is also plotted (Fig. 13C). As reported by Huang and Nanson (2007), the optimum width/depth ratio ς for multiple channels becomes less, reducing from 3650 for one aggregate channel to 655 for each of the five channels.

Figs. 14A and B show the total width/depth ratio of the whole anabranching system. Fig. 14B is a close-up view at the maximum sediment discharge. Similar to Huang and Nanson (2007), at the optimum state where sediment discharge reaches the maximum value, the total ς for a whole anabranching system is larger than for a single channel. The maximum sediment discharge for a single channel reduces slightly from 0.1787 to 0.1782 $m^3\ s^{-1}$ for five channels (a reduction of only 0.28%)

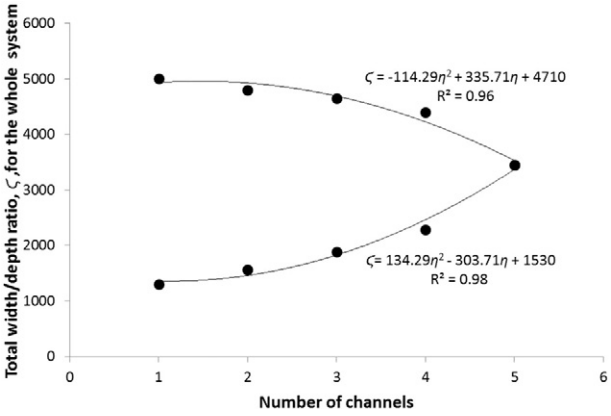

Fig. 15. Variation of the number of channels η and the width/depth ratio ς for the same amount of sediment transport. The empirical polynomial functions demonstrate the general trend of data convergence on a value of $\eta = 5$ when $\varsigma = 3450$ and $Q_s = 0.1782\ m^3\ s^{-1}$. $Q = 7530\ m^3\ s^{-1}$, $S = 0.00028$, and $d_{50} = 0.18$ mm.

while the equilibrium aggregate ς increases from 2650 to 3300 (24%). The dashed line in Fig. 14B illustrates the number of channels corresponding with their total ς with the same amount of sediment transported. The trend of ς as a function of η along the pecked line in Fig. 14B is illustrated in Fig. 15. Also similar to Huang and Nanson (2007), a multiple channel system has a lower total width/depth ratio than a single channel system with the same amount of transported sediment.

Consequently, hypothesis (2), that the channel network will approach an optimum configuration to transfer the imposed fluid and sediment loads down system, is supported by the analyses above.

5. Discussion

The Indus is a complex sand-bed channel network with elements of stochastic behaviour, but nevertheless network properties are to some extent predictable. The network expands only slightly from the dry season to the wet season from four to five channels which implies that <~25% additional monsoon water is conveyed in the additional channel, with any excess water being stored or transported overbank (Fig. 9). Bankline retreat occurs for all competent discharges greater than ca. 6000 $m^3\ s^{-1}$ but tends to be countered to a lesser extent by point bar extension on the opposing bank. As noted in many other rivers (Buraas et al., 2014), there is only a slight increase in channel capacity following large flood events (Fig. 11); and this was particularly evident in 2010 with an extension of the area of sandy point bars owing to bank erosion out-weighing bankline accretion. In this respect, hypothesis (3) is satisfied in that the channel network approaches an optimum configuration to transfer the imposed fluid and sediment loads downsystem; and so the channel network properties are insensitive to larger, if not exceptional, monsoon-induced flows. This conclusion is explored more fully below.

Thus, although channel network capacity increases when contrasting the dry season and the wet season (as it also adjusts for higher annual floods), the increase in capacity is not significant in comparison with the range of gauged flood peak discharge values. The apparent stability seems to contradict local observations of avulsion and the relatively high bankline retreat rates (e.g., 160 m per year at Alluwali) at some sections, but these indeed are *local* adjustments when compared with the reach-scale stability of the system.

It is evident that there appears to be two primary controls on the lack of channel capacity: (i) the lag time that is required for channels to adjust and (ii) the control of the regional valley slope; the latter is effectively fixed. An increase in channel capacity, including the development of new channels through avulsion (Edmonds et al., 2009), is controlled strongly by the duration of the flood event (Magilligan et al., 2015). Miori et al. (2006) noted that although an alluvial channel will widen slightly owing to a large discharge, channel narrowing post event is not physically justified to accommodate lower discharges. In the short-term, the wetted channel cross-section of lower flows will reduce within the physically larger channel; the latter remains in place and could accommodate larger flows. The fact that large monsoon floods occur annually means that there is no time available for channel capacity to reduce substantially to accommodate only a series of lower dry season discharge events. This point is illustrated by the discrepancy in the optimum ς ratio calculated using the MFE for flood flow and the observed low flow ς ratios that reflect the inevitable disequilibrium between high flow channel form and low flow conveyance. Channel narrowing can occur by local lateral deposition (Sorrells and Royall, 2014) (which is a minor response at a short timescale) during a series of lower discharge events, but the system in the short to medium term needs to await network reworking (e.g., by lateral channel migration) by monsoon floods to induce any significant adjustment to the larger channels. Nevertheless, the fact that large flood flows are substantially accommodated on the floodplains (Fig. 9) implies that the system is unable to adjust to convey large flood flows in-channel,

as has been observed for other large floods (e.g., Magilligan et al., 2015) and that extremely large floods do not necessarily change the channel or floodplain morphology (Latrubesse, 2008).

It is useful to explore this matter further with respect to the control of the valley slope. Although the river cannot readily increase its regional slope, imposition of the barrage at Taunsa (1958) has caused substantial bed aggradation (Sinha, 2010; Gaurav et al., 2011) and a reduced bed slope over the length of the backwater reach. Provided with sufficient information on surface water levels throughout the study reach, the backwater length L_b could be calculated accurately (e.g., Chow, 1959) but here may be approximated using simple trigonometry as

$$L_b = {}^{D_b}/_{S} \quad (5)$$

where D_b, the near-bankfull depth, is <13 m and S is 0.00024 to 0.00028 as defined in Section 2. Using these values the maximum backwater length is between 46 and 56 km, which compares well with the estimate of 45 km obtained from Fig. 12, wherein channel narrowing and presumed concomitant bed aggradation were noted upstream of the barrage. Substituting the barrage height (7.925 m) as h_b into Eq. 5, to replace the bankfull depth, the backwater length is between 28 and 33 km. In either case, there should have been a reduction in the channel gradient within the backwater length. The application of the Huang and Nanson (2007) MFE demonstrates the control that the imposed regional slope has on the potential evolution of channel networks with additional capacity (Huang and Nanson, 2007). Reducing the regional slope in Eq.(2) demonstrates a significant reduction in sediment transport capacity and an expected increase in ς and η. At the same time, any increase in the number of channels in the reach would also be associated with a reduction in sediment transport efficiency (Huang and Nanson, 2007) as is evident in Fig. 14B. Thus, backwater sedimentation (Millar, 2005) should induce avulsion (Mohrig et al., 2000) to form additional channels in the network although the precise controls remain uncertain (Ganti et al., 2014). Notably (see Section 3), the Huang and Nanson (2007) MFE procedure considers only channel adjustments due to changes in bedload flux. The estimate of the optimum quantity of sediment transported as bedload (Fig. 14A) during a monsoon flood discharge using the MFE produces a result that is around 3 to 4% of the estimated total annual load of suspended sediment. This value may be an underestimate of the bedload, for example Radecki-Pawlik et al. (2014) calculated 15% just upstream of the delta, but the percentage is consistent with the generally low rates of bedload transport as a fraction of the total load reported for large sand bedded rivers that carry high concentrations of suspended materials (Turowski et al., 2010). Thus, considerable suspended sediment may be depositing in the backwater reach, accelerating local channel change. The long-term effects of barrage construction are difficult to assess because of the lack of detailed data on pre-barrage channel network topology.

Nevertheless, despite the imposition of barrages several decades ago, the Indus River network (at the full reach-scale investigated in this study) remains a near-equilibrium system that is conveying water and sediment most efficiently. Reach-scale gradient increase would be required to increase conveyance, but this is not an engineering option. So, once the optimality of the network is recognized, in that multiple channels are necessary to transfer the annual flux of water and sediment, it makes economic sense to provide the rivers with sufficient space to continue to transfer the fluid discharge and the imposed sediment load towards the ocean. Sinha (2010) and Gaurav et al. (2011) noted a significant levée failure upstream of Taunsa during the peak of the 2010 discharge event and recognized that aggradation caused by the Taunsa barrage was putting levées increasingly at risk of failure, in part because engineering works encroach closely on the river macrochannel (Gaurav et al., 2011). In this latter respect, the study reach is also subject to the risk of engineering-induced avulsions as was noted by Syvitski and Brackenridge (2013) for the lower course of the Indus River below the Sukkur barrage. Constructing embankments at a sufficient distance from the channel network could prevent extensive inundation of floodplain areas without impeding the function of the channel network significantly. Such an approach, requiring modelling studies, would reduce capital investment in local river training works that, most often, are placed adjacent to, or within, the existing channel network and which fail on a regular basis. As the discharge and the sediment flux are modified anthropogenically, or by natural climate change, the space required by the river could be reviewed. Fluvial adjustments in the lower reaches of this large river are sufficiently buffered to allow informed management solutions to be applied successfully to deal with emerging channel control issues as human pressures and climate changes demand.

6. Conclusions

Aspects of the planform behaviour of the middle reaches of the Indus River in Pakistan, between Chashma and Taunsa, are predictable. The multichannel river is typified by between 2 and 11 channels at any cross-section, with on average four channels active during the dry season and five during the monsoon. Thus, the expansion of the network during the monsoon is slight and is owing to reoccupation of channels that are dry during low flows. Thus, the network structure, if not its detailed planform, is relatively stable year to year.

No significant bank erosion occurs for peak annual discharge values of <6000 $m^3\ s^{-1}$. The bank line recession is a linear function of the annual peak discharge up to at least 20,000 $m^3\ s^{-1}$, but vegetated land lost because of sand deposition on the floodplain is disproportionately large for exceptional floods such as the 2010 flood of 27,100 $m^3\ s^{-1}$. Despite some channel widening caused by high annual monsoon peak discharges, there was no significant change in the character of the channel pattern following the 2010 flood.

Application of the Huang and Nanson Maximum Flow Efficiency principle demonstrates that the river channel network is relatively insensitive to the monsoon floods, as it maintains a network that is in near-equilibrium with the mean annual flood flow of 7530 $m^3\ s^{-1}$. This conclusion pertains because the decadal timescale for adjustment of the network is much longer than the timescale of the monsoon hydrograph, with the annual excess water being stored and transported across floodplains rather than being conveyed in enlarged channels. The analysis explains the lack of significant channel adjustment following the largest recorded flood in 40 years. Major overbank flows will persist in future high-flow events. Consequently, for effective river management, floodwater and sediment needs accommodation space on protected floodplains, or alternatively, major water and sediment diversion schemes upstream of Chashma would be necessary to limit extensive floodplain inundation in the reach extending to Taunsa.

The findings of this paper are a starting point for consideration of flood risk and the impact on the population of the river corridor of the Indus. The mechanism by which high river discharge impacts on the rural population can be considered in two key domains: first the loss of river bank through erosion and second through the sustained inundation of residential and agricultural production areas (Sharma et al., 2010). Bank erosion can result in permanent displacement whereas inundation, assuming heavy deposition of sands is avoided, does not necessarily lead to long-term depopulation. Indeed there are some fertility benefits associated with flooding that are, of course, heavily offset by negative impacts in the case of severe flooding. The finding of this work is significant from the perspective of flood recovery planning as it identifies the potential to develop detailed flood exposure and risk maps and the associated need to prioritize flood protection, land rehabilitation, and the development of temporary refugia in contrast to the permanent displacement associated with erosive loss of land and the social disruption and conflict that are typical of such displacements.

Acknowledgements

The project was made possible through funding provided by FAO contract reference no. LoA/TF/PAK/2011/TCESP. The manuscript was written by PAC during tenure of a Chinese Academy of Science President's International Visiting Fellowship in Beijing, China, in 2015 and in Kaifeng, China, in 2016. The contribution of S. E. Darby to this paper was supported in part by award NE/JO21970/1 from the UK Natural Environment Research Council (NERC). Especial thanks are owed to John Latham, Senior Environment Officer, NRL, FAO, for enthusiastic support for the project. All data used in the analyses are available upon request. Requests should be sent in the first instance to the first author. Edgardo Latrubesse and Gerald Nanson are thanked for their incisive reviews which contributed to the final presentation of this paper.

References

Ali, A., 2013. Indus Basin Floods: Mechanisms, Impacts and Management. Asian Development Bank, Mandaluyong City, Philippines, p. 55.
Bettess, R., White, W.R., 1983. Meandering and braiding of alluvial channels. Proceedings of the Institution of Civil Engineers Part 2 75, 525–538.
Bhatti, A., Suttinon, P., Nasu, S., 2011. Monitoring spatial and temporal variability of suspended sediment in Indus River by means of remotely sensed data. Annals of GIS 17 125–13. https://doi.org/10.1080/19475683.2011.576267.
Bolla Pittaluga, M., Repetto, R., Tubino, M., 2003. Channel bifurcation in braided rivers: equilibrium configurations and stability. Water Resour. Res. 39:1046. https://doi.org/10.1029/2001WR001112.
Bull, W.B., 1991. Geomorphic Responses to Climatic Change. Oxford Press, Oxford, U. K. and New York, p. 326.
Buraas, E.M., Magilligan, F.J., Renshaw, C.E., Dade, W.B., 2014. Impact of reach geometry on stream channel sensitivity to extreme floods. Earth Surf. Process. Landf. 39: 1778–1789. https://doi.org/10.1002/esp.3562.
Carling, P.A., Jansen, J., Meshkova, M., 2013. Multichannel rivers: their definition and classification. Earth Surf. Process. Landf. 39, 26–37.
Chatfield, C., 1996. The Analysis of Time Series. 5th edn. London, Chapman and Hall, p. 283.
Chow, V.T., 1959. Open-channel Hydraulics. McGraw Hill, New York, p. 680.
Clift, P.D., 2002. A Brief History of the Indus River. Geol. Soc. Lond., Spec. Publ. 195, 237–258.
Clift, P.D., Giosan, L., 2013. Sediment fluxes and buffering in the post-glacial Indus Basin. Basin Res. 25:1–18. https://doi.org/10.1111/bre.12038.
Costa, J.E., O'Connor, J.E., 1995. Geomorphically effective floods. In: Costa, J.E. (Ed.), Natural and Anthropogenic Influences in Fluvial Geomorphology, Geophysical Monograph 89. American Geophysical Union, pp. 45–56.
Crosato, A., Mosselman, E., 2009. Simple physics-based predictor for the number of river bars and the transition between meandering and braiding. Water Resour. Res. 45. https://doi.org/10.1029/2008WR007242.
Dade, W.B., Friend, P.F., 1998. Grain size, sediment-transport regime and channel slope in alluvial rivers. J. Geol. 106:661–675. https://doi.org/10.1086/516052.
Darby, S.E., Trieu, H.Q., Carling, P.A., Sarkkula, J., Koponen, J., Kummu, M., Conlan, I., Leyland, J., 2010. A physically based model to predict hydraulic erosion of fine-grained river-banks: the role of form roughness in limiting erosion. J. Geophys. Res. 115 F04003. https://doi.org/10.1029/2010JF001708.
Eaton, B.C., Millar, R.G., Davidson, S., 2010. Channel patterns: Braided, anabranching, and single-thread. Geomorphology 120:353–364. https://doi.org/10.1016/j.geomorph.2010.04.010.
Edmonds, D.A., Hoyal, D.C.J.D., Sheets, B.A., Slingerland, R.L., 2009. Predicting delta avulsions: Implications for coastal wetland restoration. Geology 37:759–762. https://doi.org/10.1130/G25743A.1.
Evans, J.E., Huxley, J.M., Vincent, R.K., 2007. Upstream channel changes following dam construction and removal using a GIS/remote sensing approach. J. Am. Water Resour. Assoc. 43:683–697. https://doi.org/10.1111/j.1752-1688.2007.00055.x.
Ganti, V., Chu, Z., Lamb, M.P., Nittrouer, J.P., Parker, G., 2014. Testing morphodynamic controls on the location and frequency of river avulsions on fans versus deltas: Huanghe (Yellow River), China. Geophys. Res. Lett. 41:7882–7890. https://doi.org/10.1002/2014GL061918.
Gares, P.A., Sherman, D.J., Nordstrom, K.P., 1994. Geomorphology and natural hazards. Geomorphology 10:1–18. https://doi.org/10.1016/0169-555X(94)90004-3.
Gaurav, K., Sinha, R., Panda, P.K., 2011. The Indus flood of 2010 in Pakistan: a perspective analysis using remote sensing data. Nat. Hazards 59:1815–1826. https://doi.org/10.1007/s11069-011-9869-6.
Gilmartin, D., 2015. Blood and Water: The Indus River in Modern History. University of California Press, Oakland, California, p. 376.
Gupta, H., Shuh-Ji Kao, S.-J., Dai, M., 2012. The role of mega dams in reducing sediment fluxes: a case study of large Asian rivers. J. Hydrol. 464-465:447–458. https://doi.org/10.1016/j.jhydrol.2012.07.038.
Hamilton, J.D., 1994. Time Series Analysis. Princeton University Press, Princeton, NJ (674 + pp).
Haq, I.U., 2013. Sediment management of Tarbela reservoir. 72nd Annual Session of Pakistan Engineering Congress. Pakistan Engineering Congress, Lahore, pp. 19–42.
Huang, H.Q., 2010. Reformulation of the bed load equation of Meyer-Peter and Müller in light of the linearity theory for alluvial channel flow. Water Resour. Res. 46 W09533. https://doi.org/10.1029/2009WR008974 (2010).
Huang, H.Q., Nanson, G.C., 2007. Why some alluvial rivers develop an anabranching pattern. Water Resour. Res. 43 W07441. https://doi.org/10.1029/2006WR005223.
Inam, A., Clift, P.D., Giosan, L., Tabrez, A.R., Tahir, M., Rabbani, M.M., Danish, M., 2007. The geographic, geological and oceanographic setting of the Indus River. In: Gupta, A. (Ed.), Large Rivers: Geomorphology and Management. John Wiley and Sons, Chichester:pp. 333–346 https://doi.org/10.1002/9780470723722.ch16.
Kale, V.S., 2014. Is flooding in South Asia getting worse and more frequent? Singap. J. Trop. Geogr. 35:161–178. https://doi.org/10.1111/sjtg.12060.
Khan, B., Iqbal, M.J., Yosufzai, M.A.K., 2011. Flood risk assessment of River Indus of Pakistan. Arab. J. Geosci. 4:115–122. https://doi.org/10.1007/s12517-009-0110-9.
Kirmani, S.S., 1962. Sediment problems in the Indus basin, in Sediment Problems as a Result of Indus Basin Works. Symposium of Pakistan Engineering Congress. VI. Pakistan Engineering Congress, Lahore (pp. 69-104 plus figures).
Kleinhans, M.G., Jagers, H., Mosselman, E., Sloff, C., 2008. Bifurcation dynamics and avulsion duration in meandering rivers by one-dimensional and three-dimensional models. Water Resour. Res. 44. https://doi.org/10.1029/2007WR005912.
Kondolf, G.M., 1997. Hungry water: effects of dams and gravel mining on river channels. Environ. Manag. 21:533–551. https://doi.org/10.1007/s002679900048.
Laghari, A.N., Vanham, D., Rauch, W., 2012. The Indus basin in the framework of current and future water resources management. Hydrol. Earth Syst. Sci. 16:1063–1083. https://doi.org/10.5194/hess-16-1063-2012.
Latrubesse, E.M., 2008. Patterns of anabranching channels: the ultimate end-member adjustment of mega rivers. Geomorphology 101:pp. 130–145. https://doi.org/10.1016/j.geomorph.2008.05.035.
Magilligan, F.J., Buraas, E.M., Renshaw, C.E., 2015. The efficacy of stream power and flow duration on geomorphic responses to catastrophic flooding. Geomorphology 228: 175–188. https://doi.org/10.1016/j.geomorph.2014.08.016.
Meshkova, L.V., Carling, P.A., 2013. Discrimination of alluvial and mixed bedrock–alluvial multichannel river networks. Earth Surf. Process. Landf. 38:1299–1316. https://doi.org/10.1002/esp.3417.
Meyer-Peter, E., Müller, R., 1948. Formulas for Bed-load Transport, Paper Presented at 2nd IAHR Meeting. International Association of Hydraulic Engineering and Research, Stockholm, pp. 39–64.
Millar, R.G., 2005. Theoretical regime equations for mobile gravel-bed rivers with stable banks. Geomorphology 64:207–220. https://doi.org/10.1016/j.geomorph.2004.07.001.
Milliman, J.D., Quraishee, G.S., Beg, M.A.A., 1984. Sediment discharge from the Indus River to the ocean: past, present and future. In: Haq, B.U., Milliman, J.D. (Eds.), Marine Geology and Oceanography of Arabian Sea and Coastal Pakistan. Van Nostrand Reinhold, New York, pp. 5–70.
Miori, S., Repetto, R., Tubino, M., 2006. A one-dimensional model of bifurcations in gravel bed channels with erodible banks. Water Resour. Res.:42 https://doi.org/10.1029/2006WR004863.
Mohrig, D., Heller, P.L., Paola, P., Lyons, W.J., 2000. Interpreting avulsion process from ancient alluvial sequences: Guadalope-Matarranya system (northern Spain) and Wasatch Formation (western Colorado). Geol. Soc. Am. Bull. 112:1787–1803. https://doi.org/10.1130/0016-7606.
Nanson, G.C., Huang, H.Q., 2017. Self-adjustment in rivers: evidence for least action as the primary control of alluvial-channel form and process. Earth Surf. Process. Landf. 42: 575–594. https://doi.org/10.1002/esp.3999.
Nicholas, A., 2013a. Morphodynamic diversity of the world's largest rivers. Geology 41: 475–478. https://doi.org/10.1130/G34016.1.
Nicholas, A., 2013b. Modelling the continuum of river channel patterns. Earth Surf. Process. Landf. 38:1187–1196. https://doi.org/10.1002/esp.3431.
van Niekerk, A.W., Heritage, G.L., Moon, B.P., 1995. River classification for management: the geomorphology of the Sabie River in the eastern Transvaal. S. Afr. Geogr. J. 77: 68–76. https://doi.org/10.1080/03736245.1995.9713594.
Pizzuto, J., Keeler, J., Skalak, K., Karwan, D., 2017. Storage filters upland suspended sediment signals delivered from watersheds. Geology 45:151–154. https://doi.org/10.1130/G38170.1.
Radecki-Pawlik, A., Laszek, W., Plesiński, K., Lashari, B.K., 2014. Dominate discharge in the Indus River from downstream of the Kotri barrage dam. Acta Sci. Pol. Form. Circum. 13:225–232. https://doi.org/10.15576/ASP.FC/2014.13.4.225.
Rehman, S.S., Sabir, M.A., 1996. Spatio-temporal variation in the suspended load rivers of NWFP, Pakistan. Peshawar University Teachers' Assocation Journal 3, 133–142.
Sabir, M.A., Shafiq-Ur-Rehman, S., Umar, M., Waseem, A., Farooq, M., Khan, A.R., 2013. The impact of suspended sediment load on reservoir siltation and energy production: a case study of the Indus River and its tributaries. Pol. J. Environ. Stud. 22, 219–225.
Samuels, P.G., 1990. Cross section location in one-dimensional models. In: White, W.R. (Ed.), Proceedings of an International Conference on River Flood Hydraulics. Wiley, Chichester, U.K., pp. 339–350.
Sear, D.A., 2004. Bedload yield measurements with load cell bed load traps and prediction of bed load yield from hydrograph shape. In: Bogen, J., Walling, D.E. (Eds.), Erosion and Sediment Transport Measurements in Rivers: Technological and Methodological Advances. IAHS, Wallingford, U.K., pp. 146–153.
Sharma, N., Johnson, F.A., Hutton, C.W., Clark, M.J., 2010. Hazard, vulnerability and risk on the Brahmaputra basin: a case study of river bank erosion. Open Journal of Hydrology 4, 211–226.
Singh, P., Bengtsson, L., 2004. Hydrological sensitivity of a large Himalayan basin to climate change. Hydrol. Process. 18:2363–2385. https://doi.org/10.1002/hyp.1468.
Sinha, R., 2010. A river runs through it. Public Service Review: International Development 17, 20–22.

Song, C., Woodcock, C.E., Seto, K.C., Lenney, M.P., Macomber, S.A., 2001. Classification and change detection using Landsat TM data: when and how to correct atmospheric effects? Remote Sens. Environ. 75:230–244. https://doi.org/10.1016/S0034-4257(00)00169-3.

Sorrells, R.M., Royall, D., 2014. Channel bifurcation and adjustment on the upper Yadkin River, North Carolina (USA). Geomorphology 223:33–44. https://doi.org/10.1016/j.geomorph.2014.06.020.

Syvitski, J.P.M., Brackenridge, G.R., 2013. Causation and avoidance of catastrophic flooding along the Indus River, Pakistan. GSA Today 23 (1):1–10. https://doi.org/10.1130/GSATG165A1.

Syvitski, J.P.M., Kettner, A.J., Overeem, I., Giosan, L., Brakenridge, G.R., Hannon, M., Bilham, R., 2013. Anthropocence metamorphosis of the Indus Delta and lower floodplain. Anthropocene 3, 24–35 (doi:10.1016 j.ancene.2014.02.003).

Turowski, J.M., Rickenmann, D., Dadson, S.J., 2010. The partitioning of the total sediment load of a river into suspended load and bedload: a review of empirical data. Sedimentology 57:1126–1146. https://doi.org/10.1111/j.1365-3091.2009.01140.x.

Vita-Finzi, C., 2012. River history. Phil. Trans. R. Soc. A 370:2029–2039. https://doi.org/10.1098/rsta.2011.0604.

Walton, B., 2010. Pakistan and India in Dam Building Race – Interpreting the Indus Waters Treaty, November 30th, 2010. http://www.circleofblue.org, Accessed date: 11 November 2016.

Winston, W., Yang, Y.-C., Savitsky, A., Alford, D., Brown, C., Wescoat, J., Debowicz, D., Robinson, S., 2013. The Indus Basin of Pakistan: The Impacts of Climate Risks on Water and Agriculture. World Bank Publications, p. 184.

Wong, M., Parker, G., 2006. Reanalysis and correction of bed-load relation of Meyer-Peter and Müller using their own database. J. Hydraul. Eng. 132:1159–1168. https://doi.org/10.1061/(ASCE)0733-9429(2006)132:11(1159.

Yalin, M.S., 1977. Mechanics of Sediment Transport. 2nd Edition. Pergamon Press, Oxford, UK, p. 295.

Young, G.J., Hewitt, K., 1990. Hydrology research in the upper Indus basin. In: Molnar, L. (Ed.), Hydrology of Mountainous Areas, Proceedings of the Štrbské Pleso Workshop, Czechoslovakia, June 1988. IAHS Publ 190, pp. 139–152.